Rare Metal Materials and Engineering
Volume 51, Issue 7, July 2022
Available online at www.rmme.ac.cn

Science Press

Cite this article as: Zhou Chen, Lin Jinbao, He Wenhui, et al. Tensile Deformation Simulation of Extruded ZK60 Alloy by VPSC Model[J]. Rare Metal Materials and Engineering, 2022, 51(07): 2429-2435.

ARTICLE

Tensile Deformation Simulation of Extruded ZK60 Alloy by VPSC Model

Zhou Chen[1], Lin Jinbao[1], He Wenhui[1], Mu Weipeng[2], Liu Erqiang[1]

[1] School of Applied Science, Taiyuan University of Science and Technology, 030024 Taiyuan, China; [2] School of Materials Science and Engineering, Taiyuan University of Science and Technology, 030024 Taiyuan, China

Abstract: The initiation condition for deformation mechanism of extrusion AZ60 Mg alloy during tensile deformation along different directions at room temperature was investigated through experiments and visco-plastic self-consistent (VPSC) modeling, and the relationship between the deformation mechanism with the flow curves, texture evolutions, and microstructure of ZK60 Mg alloys was also analyzed. By adjusting the parameters in VPSC model, the crystal plastic mechanics model with slip coupled with twin was established. The differences in texture evolution during tension along different directions were compared, and the influence of deformation mechanism on the yield asymmetry was analyzed. The experiment and simulation results show that due to the initiation of $\{10\bar{1}2\}$ twin, most grains are rotated at a large angle (about 90°) when the tensile direction is perpendicular to the extrusion direction, namely PED. The prismatic <*a*> slip is the main deformation mode resulting in the yield asymmetry of ZK60 alloy during tensile deformation along different directions. When the ZK60 alloys are under tensile deformation along extrusion direction (ED), due to the preferential orientation, the $\{10\bar{1}1\}$ twin is difficult to initiate and the higher yield strength can be obtained. The yield stress under tension along the direction with an angle of 45° to ED is higher than along PED. As the tensile stress gradually increases, the prismatic <*a*> slip is gradually initiated, resulting in the higher stress curves along PED than those along the direction with an angle of 45° to ED.

Key words: ZK60 alloy; visco-plastic self-consistent (VPSC) model; yield asymmetry; deformation mechanisms; tension

Magnesium (Mg) alloy is featured by the advantages of low density, high specific strength, and high specific stiffness. It has broad application prospects in the fields of aerospace and transportation[1-3]. Due to the difference in initial crystal orientation, Mg alloys exhibit the distinct anisotropy of mechanical properties, such as ductility and strain hardening[4-11]. However, the mechanics anisotropy of Mg alloys should be ameliorated for the wider application. Due to its hexagonal close-packed (hcp) crystal structure, Mg alloy has few slip systems and thereby the unsatisfied formability and ductility at room temperature[12-14], which seriously reduces the production sufficiency and increases the production cost. Moreover, the critical resolved shear stress (CRSS) of each slip and twin is different. In addition, the Mg alloy can easily produce a strong fiber texture on (0002) plane which is parallel to the extrusion direction (ED) during the treatment processes[15], resulting in obvious mechanical anisotropy.

The Mg alloys have different deformation modes, resulting from the four types of slip systems and two types of twin systems, such as basal <*a*> slip, prismatic slip, pyramidal <*a*> slip, pyramidal <*c*+*a*> slip, extension twin, and contraction twin[16-18]. The grain orientations and the strain path of the Mg alloy during deformation are closely related to the slip and twin motions[19-24]. The twin can be easily activated in the initial deformation stage of Mg alloy[25], and that with severe directionality can coordinate the strain along the *c*-axis direction to influence the slip initiation, which hence affects the strain hardening and softening behavior of Mg alloys. Therefore, the twin is vital in the deformation process of Mg alloys[26-30].

In recent years, the visco-plastic self-consistent (VPSC) model has been widely used to simulate the mechanical responses, texture evolutions, and crystallographic

Received date: July 23, 2021
Foundation item: National Natural Science Foundation of China (51574171); Natural Science Foundation of Shanxi Province (201901D11126)
Corresponding author: Lin Jinbao, Ph. D., Professor, School of Applied Science, Taiyuan University of Science and Technology, Taiyuan 030024, P. R. China, Tel: 0086-351-6998165, E-mail: linjinbao@qq.com

characteristics. Lin et al[31] used VPSC model to study the asymmetry and work hardening behavior of extruded AZ31 Mg alloy under uniaxial compression and tension. Chen et al[32] revealed that VPSC model is very useful to study the plastic deformation behavior of Mg alloys.

The uniaxial tension and compression of extruded Mg alloys are widely discussed, but the tension status of Mg alloys along different directions is rarely investigated. Therefore, the relationship between texture evolutions and deformation modes during the tensile deformation along different directions as well as the origination of the yield asymmetry of ZK60 Mg alloys was investigated in this research. VPSC model was employed to simulate the flow curves, texture evolutions, and deformation modes of the as-extruded ZK60 Mg alloys under tension along different directions at room temperature. Through adjusting the parameters of VPSC model, the crystal plastic mechanics model with slip coupled with twin was established. The experiments and established VPSC model were both employed to analyze the texture evolutions and the activities of basal slip, prismatic slip, pyramidal slip, extension twin, and contraction twin in alloys during the tensile deformation. This research revealed the yield asymmetry mechanism, provided practical guidance for the development of high-performance structural materials of wrought Mg alloys, and broadened the industrial applications of Mg alloys.

1 Experiment and Constitutive Model Establishment

The raw material was the commercially hot-extruded ZK60 (Mg-5.5Zn-0.5Zr, wt%) alloy bar with a diameter of 30 mm and a basal fiber texture, which mainly contains the {0002} basal plans and the <10$\bar{1}$0> direction parallel to ED. The Philips PW1820 X-ray diffractometer (XRD) was used at the working voltage of 40 kV and current of 40 mA. The metallographic observations were conducted on LEICA DM 2700M optical microscope (OM). The gauge length of the tensile specimen was 10 mm×3 mm×1.5 mm, and the mechanical performance was tested at room temperature using the WDW-E100D electronic universal testing machine with the strain-rate of $\dot{\varepsilon}$=5×10^{-4} s^{-1}. To ensure the accuracy of the experiment, the initial wire cutting specimen was pre-polished with 400#~800# sandpaper. After the tensile test, the tensile specimens were cut along ED for the microstructure observation. Fig. 1 shows the schematic diagram of the extruded ZK60 alloy specimen and different directions of tensile deformation. The 45ED indicates the tensile direction with an angle of 45° to ED; PED indicates the tensile direction perpendicular to ED.

The VPSC model has been studied[33-35] and used. The interaction between the grains is very important in this model. It is assumed that the grains are elliptical inclusions in an infinite homogeneous equivalent medium.

The visco-plastic constitutive behavior of grains can be expressed by the non-linear rate-sensitivity equation[36], as follows:

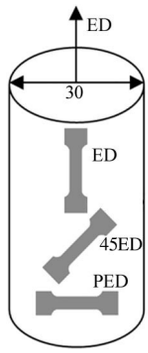

Fig.1 Schematic diagram of extruded ZK60 alloy and different directions of tensile deformation

$$\varepsilon_{ij}(\bar{x}) = \sum_{\mathrm{S}} m_{ij}^{\mathrm{S}} \gamma^{\mathrm{S}}(\bar{x}) = \gamma_0 \sum_{\mathrm{S}} m_{ij}^{\mathrm{S}} \left\{ \frac{m_{kl}^{\mathrm{S}} \sigma_{kl}(\bar{x})}{\tau^{\mathrm{S}}} \right\}^n \tag{1}$$

where $\varepsilon(\bar{x})$ and $\sigma(\bar{x})$ are the deviatory strain rate and stress, respectively; the subscripts i, j, k, and l are variable positive integer; the subscript or superscript S represents the slip/twin system; τ^{S} and $m_{ij}^{\mathrm{S}} = \frac{1}{2}\left(n_i^{\mathrm{S}} b_j^{\mathrm{S}} + n_j^{\mathrm{S}} b_i^{\mathrm{S}}\right)$ are the threshold stress and the symmetric Schmid tensor of slip/twin system, respectively (n^{S} and b^{S} are the normal vector and Burgers vector of the slip/twin systems, respectively); γ^{S} is the shear rate with $\gamma^{\mathrm{S}} = \gamma_0 \left(\frac{m_{kl}^{\mathrm{S}} \sigma_{kl}(\bar{x})}{\tau^{\mathrm{S}}} \right)^n$; γ_0 is a normalization factor; n is the rate sensitivity exponent. Besides, τ^{S} also indicates the critical shear stress of deformation mechanism, determining the initiation of deformation mechanism. Thus, Eq.(1) can be described by the Voce hardening model[36], as follows:

$$\tau^{\mathrm{S}} = \tau_0^{\mathrm{S}} + \left(\tau_1^{\mathrm{S}} + \theta_1^{\mathrm{S}} \Gamma\right)\left[1 - \exp\left(- \Gamma \left| \frac{\theta_0^{\mathrm{S}}}{\tau_1^{\mathrm{S}}} \right| \right)\right] \tag{2}$$

where τ_0^{S} and $\tau_0^{\mathrm{S}} + \tau_1^{\mathrm{S}}$ are the initial CRSS and the back-extrapolated CRSS, respectively; θ_0^{S} and θ_1^{S} are the initial and asymptotic hardening rates of mechanisms, respectively; Γ is the accumulated shear in the grain. Thus, Γ can be expressed by Eq.(3), as follows:

$$\Gamma = \sum_{\mathrm{S}} \Delta\gamma^{\mathrm{S}} \tag{3}$$

Two main deformation mechanisms are considered in the VPSC model establishment[34]. The predominant twin reorientation (PTR) was used in Ref. [37], which records the shear strain γ^{t} contributed by each twin system (t) and the associated volume fraction $V^{\mathrm{t,g}} = \gamma^{\mathrm{t,g}}/S^t$ in each grain (g)[36,37] (S is the characteristic twin shear). The cumulative number of the volume fraction of twin can be expressed, as follows:

$$V^{\mathrm{acc,mode}} = \sum_{\mathrm{g}} \sum_{\mathrm{t}} V^{\mathrm{t,g}} \tag{4}$$

where $V^{\mathrm{t,g}}$ is the volume fraction of twin. $V^{\mathrm{th,mode}}$ indicates the redirection threshold value, which is defined by Eq. (5), as follows:

$$V^{\mathrm{th,mode}} = A^{\mathrm{th1}} + A^{\mathrm{th2}} \frac{V^{\mathrm{eff,mode}}}{V^{\mathrm{acc,mode}}} \tag{5}$$

where A^{th1} and A^{th2} are two material constants; $V^{\mathrm{eff,mode}}$ is the

effective twin fraction. After each incremental step, the grains are randomly selected, and the twin system with the highest cumulative volume fraction is determined. When $V^{acc,mode}$ is larger than the $V^{th,mode}$, the grains are allowed to reorient, and $V^{eff,mode}$ and $V^{th,mode}$ will be updated. This procedure is repeated until the effective twin volume fraction exceeds the cumulative twin volume fraction. The VPSC model is widely used to simulate and analyze the deformation mechanism and texture evolution of Mg alloys.

2 Results and Discussion

2.1 Flow curves and material parameters

The (0002) plane of ZK60 alloys parallel to ED is selected as the initial fiber texture in the VPSC simulation. Moreover, the interaction mode between crystal grains is considered to be an affine effect. The radiation stress condition is n=5 at room temperature, indicating that it is insensitive to the strain rate, and the shape of the crystal grain changes after each analysis part is finished. This VPSC model considers four types of slip system and two types of twin system. Table 1 shows the hardening constants with a matching relationship with the related parameter curves under tension along different directions. It should be noted that the hardening parameters of the VPSC model are obtained from the fitting results of experiment data. In addition, the simulated CRSS values of different deformation mechanisms can be affected by various factors, such as grain size and grain shape[17].

The experiment and the simulated tension flow curves of ZK60 alloys during tension along different directions are presented in Fig. 2, which show good agreement, inferring the simulation accuracy. As shown in Fig. 2, the yield stress along ED (287 MPa) of the extruded ZK60 alloy is much greater than that along PED (130 MPa) and along 45ED (162 MPa). The flow curves under tension all show the slow strain hardening throughout the strain stage until the specimens fracture, but the strain hardening rate is firstly fast and gradually becomes slow. The strong mechanical anisotropy and yield asymmetry can be observed in Fig. 2. The experimental mechanical properties of the ZK60 alloy under tension along different directions at room temperature are summarized in Table 2.

2.2 Evolutions of the texture

Fig. 3 illustrates the initial microstructure, measured pole figure, and VPSC simulated pole figure of the as-extruded ZK60 alloys. Fig. 3b shows the incomplete pole figure of ZK60 alloy directly measured by XRD on extrusion direction-transverse direction (TD) plane. The general features of measured texture agree well with the simulated texture results. As an extruded bar, the initial texture is the typical fiber texture, suggesting that the {0002} planes of most grains are approximately parallel to ED. When the grain shape changes during the extrusion process and the grains are tensile deformed along ED, some elongated grains can be observed. The good consistency between the measured and simulated results infers the accuracy of the simulation.

Fig. 4 shows the simulated evolutions of texture of ZK60 alloys after tensile deformation along different directions. ND indicates the normal direction. It can be seen from Fig. 4a and 4b that when the strain is increased from 6% to 12%, under the uniaxial tensile deformation, the pole figures remain in the fiber texture, and the pole figure type and intensity do not obviously change. Fig. 4c and 4d show the simulated pole figures under the strain of 8% and 16% and the tensile deformation along 45ED, respectively. It can be seen that the (0002) basal plane of the crystal grains tend to rotate along the direction perpendicular to the loading direction, and no sudden change in the orientation of the crystal grains can be observed. Fig. 4e and 4f illustrate the appearance of a large number of projections of the {0002} basal plane when the strain along PED is increased to 8% and 16%, respectively, which indicates that the grain orientation undergoes abrupt changes (approximately 90°). According to Ref. [10-14], this phenomenon should be ascribed to the initiation of twins. To clarify the effect of twins, the simulation parameters for investigation of the deformation mechanisms along PED were adjusted. Fig. 5 shows the relative activity of different deformation mechanisms of ZK60 alloys and the simulated pole figure without consideration of the $\{10\bar{1}2\}$ twin during tension along PED. It can be seen that there is no projection on the pole of the (0002) base plane.

2.3 Deformation mechanism

Fig. 6 shows the relative activity of different deformation mechanisms of ZK60 alloy along different directions. When the tensile direction is parallel to the (0002) basal planes (ED), the contraction twins enlarge. However, the high CRSS (76~153 MPa) of the contraction twins causes the shear stress below the critical value, and the contraction twin mechanism is in a closed state. Therefore, the prismatic <a> slip is the

Table 1 Simulated VPSC hardening parameters of ZK60 alloy under tension along different directions at room temperature

Deformation mode	Crystallographic type	Initial critical resolved shear stress, τ_0/MPa	Back-extrapolated critical resolved shear stress, τ_1/MPa	Initial hardening rate, θ_0/MPa	Asymptotic hardening rate, θ_1/MPa
Basal <a>	$\{0001\}\langle 11\bar{2}0\rangle$	32	15	400	120
Prismatic <a>	$\{10\bar{1}0\}\langle 11\bar{2}0\rangle$	150	0	250	0
Pyramidal <a>	$\{10\bar{1}1\}\langle 11\bar{2}0\rangle$	300	150	800	0
Pyramidal <c+a>	$\{11\bar{2}2\}\langle 11\bar{2}3\rangle$	170	300	4000	3000
Extension twin	$\{10\bar{1}2\}\langle 10\bar{1}1\rangle$	80	0	0	250
Contraction twin	$\{10\bar{1}1\}\langle 10\bar{1}2\rangle$	220	0	0	100

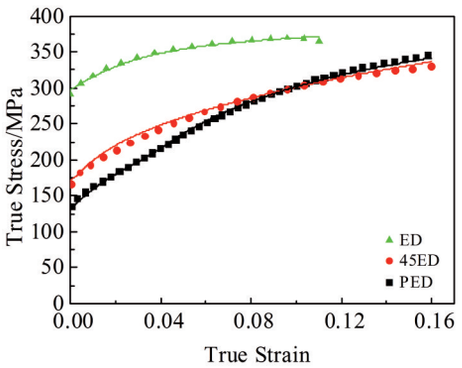

Fig.2 Experiment and simulated stress-strain curves of ZK60 alloys under tension along different directions at room temperature

Table 2 Practical mechanical properties of extruded ZK60 alloys at room temperature

Direction	Yield strength/MPa	Ultimate tensile strength/MPa	Elongation/%
ED	287	369	12.3
45ED	162	330	17.1
PED	130	350	17.9

predominant deformation mode at the beginning of deformation, and its relative activity accounts for ~0.45 (Fig. 6a). The stress variation rate has a positive relationship with the strain hardening rate: the greater the stress variation rate, the greater the strain hardening rate. As shown in Fig. 2, the strain hardening rate is gradually decreased, and the stress-strain curves gradually become stable. Fig. 7a shows the microstructure of the longitudinal section near the axial tensile fracture surface. It can be observed that there are fine recrystallized grains on the coarse twin boundary, and the twins are still in the initial structure. During the tensile deformation at room temperature, the deformation mechanism is dominated by slip, and the twin is less activated, which is consistent with the simulated results in Fig.6a.

As shown in Fig. 6b and 6c, a large number of basal <*a*> slip systems (approximately 80%) are initiated in the early stage of plastic deformation (strain of ~0.2%) along 45ED and PED, respectively. As the stress gradually increases, the relative activity of basal <*a*> slip decreases gradually, and more prismatic <*a*> slip is activated. During the whole tensile deformation along different directions, the strain hardening rate is gradually decreased with increasing the strain. In addition, the initiation of each deformation mechanism depends on whether the shear stress τ on the slip surface along the slip direction reaches the corresponding CRSS. It is known that $\tau = (F/A)\cos\phi\cos\lambda$, where F/A is the real yield strength, $\cos\phi\cos\lambda$ is the orientation factor or Schmid factor, ϕ is the angle between ND of the slip surface and the stress axis, and λ is the angle between the slip direction and the stress axis. For the tensile deformation along ED, due to the preferential orientation, the *c*-axis of the grains is in the compression state, the $\{10\bar{1}1\}$ twin is difficult to initiate, and a higher yield strength (287 MPa) can be obtained.

Compared with the basal <*a*> slip, the prismatic <*a*> slip plays an important role in the flow curves and the texture evolutions during tensile deformation. Duo to the preferential orientation distribution of grains, the basal <*a*> slip with low CRSS is difficult to initiate, the prismatic <*a*> slip with high CRSS can initiate, and the higher yield strength can be obtained during the tensile deformation alogn ED (287 MPa). The yield strength of ZK60 alloy during tension along 45ED and PED is 162 and 130 MPa, respectively. When the ZK60 alloys fail under the uniaxial tension, many contraction twins with acicular structure appear, as shown in Fig. 7a. It can also be seen that the yield stress along 45ED is higher than that along PED (Fig. 2). In the early tensile deformation stage, the basal <*a*> slip is the dominated deformation mode for tension along 45ED and PED (Fig. 6b and 6c). However, the prismatic <*a*> slip and $\{10\bar{1}2\}$ twin gradually dominate the deformation mode along 45ED and PED, respectively. The preferential orientation distribution of grains leads to the $\{10\bar{1}2\}$ twin with low CRSS, which is unable to initiate under tension along 45ED, and thereby the prismatic <*a*> slip with high CRSS is initiated. The ZK60 alloy exhibits higher yield stress under tension along 45ED than that long PED does. With increasing the tensile stress along PED, the relative activity of prismatic <*a*> slip in the alloy is gradually increased, resulting in the fact that the true stress-strain curve of ZK60 alloy during tensile deformation along PED is higher than that along 45ED at high strains. For the tensile

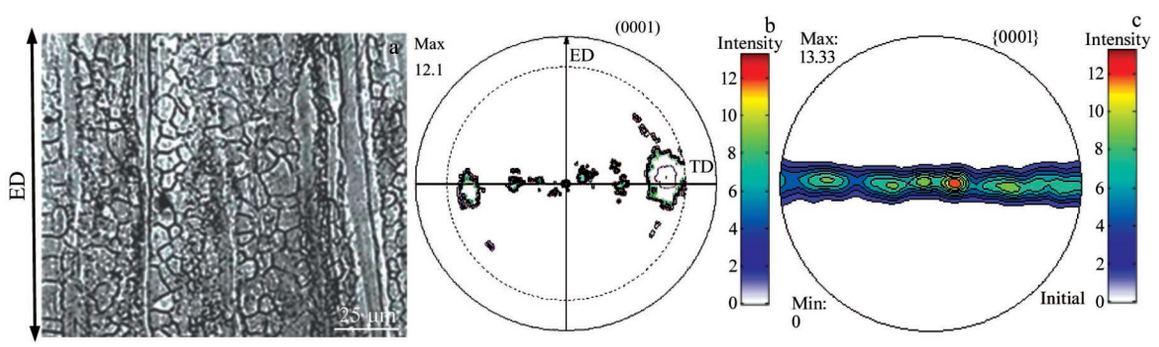

Fig.3 Cross-section microstructure (a), measured pole figure (b), and VPSC simulated pole figure (c) of as-extruded ZK60 alloy

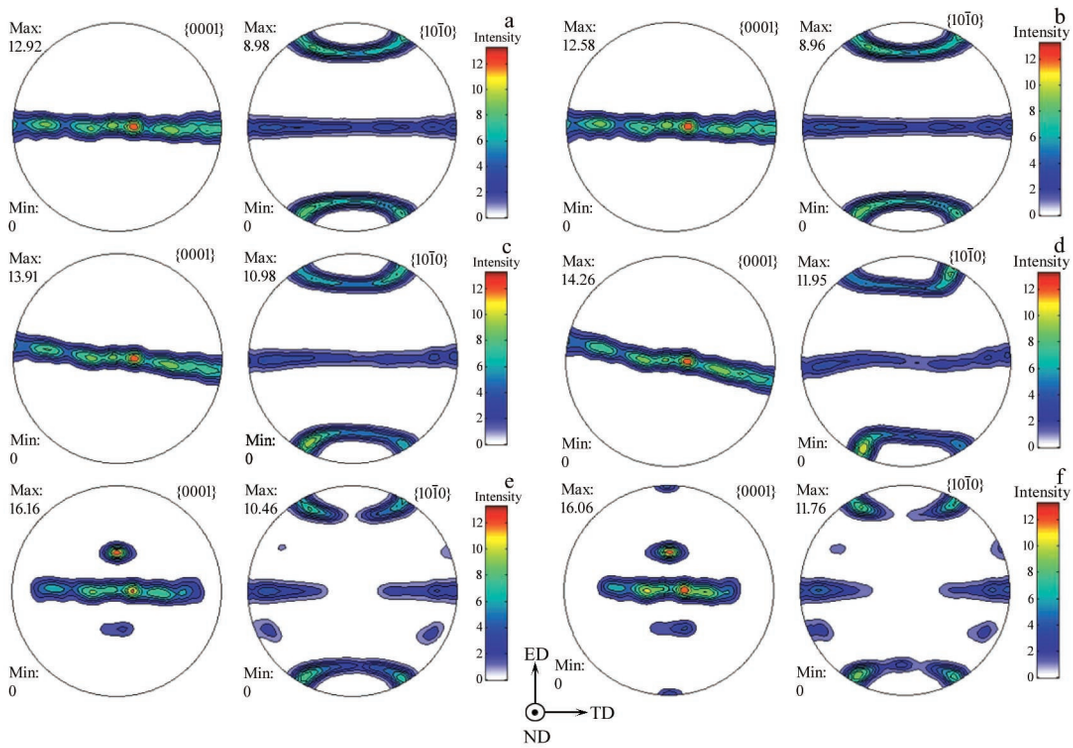

Fig.4 Simulated texture evolutions of ZK60 alloys at different strains along different directions: (a) strain of 6%-ED; (b) strain of 12%-ED; (c) strain of 8%-45ED; (d) strain of 16%-45ED; (e) strain of 8%-PED; (f) strain of 16%-PED

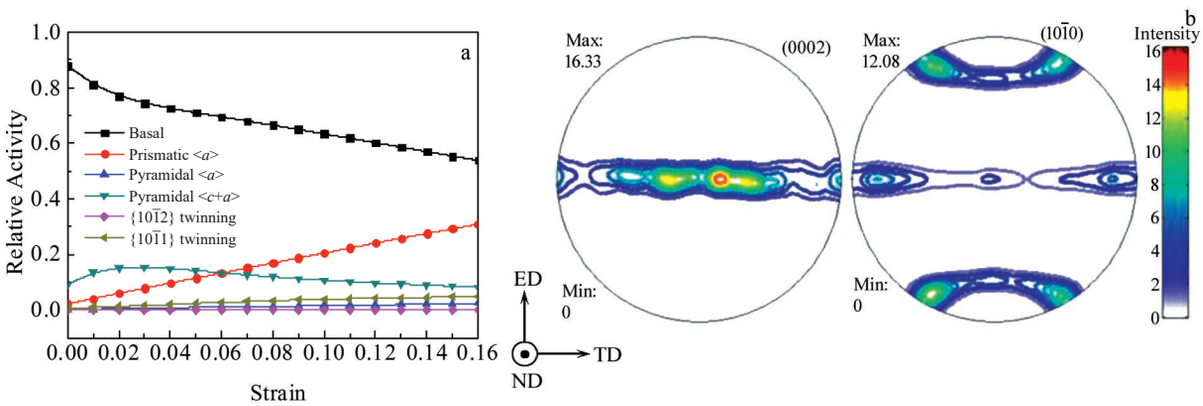

Fig.5 Relative activities of different deformation mechanisms along PED of ZK60 alloys (a); simulated pole figure with strain of 16% along PED without consideration of {10$\bar{1}$2} twin (b)

deformation along PED, the *c*-axis of the grains has an angle of 0°~30° with PED, which is favorable for {10$\bar{1}$2} twin initiation. In the early stage of tension along PED, the deformation mechanism is dominated by basal <*a*> slip coupled with {10$\bar{1}$2} twin. As shown in Fig. 7b, a small amount of coarse lenticular twin can be seen in the longitudinal section near the tensile fracture surface after tension along PED, namely the tension twin. The general characteristics of microstructures can be well explained by the relative activities of different deformation mechanisms. For tensile deformation along 45ED, as shown in Fig. 7c, the distortion occurs at the fracture, the deformation is very serious, and no obvious twins can be found, mainly because of the dislocation. These results show that the simulated results agree well with the experiment ones.

It can be seen that the true stress-strain curves, the microstructure of the tensile fracture surface, and the texture evolutions can be well explained by the relative activities of the deformation mechanisms. The prismatic <*a*> slip at the beginning of the deformation can cause obvious yield behavior, and the relative activities of basal <*a*> slip, pyramidal <*c*+*a*> slip, {10$\bar{1}$1} twin, and {10$\bar{1}$2} twin can affect the strain hardening behavior of ZK60 alloys. In addition, the pyramidal <*a*> slip is not significantly initiated

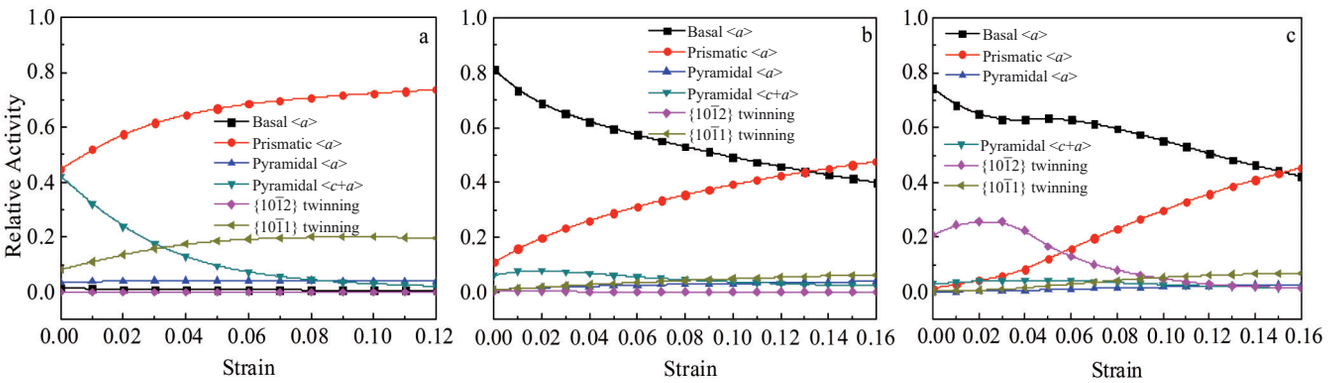

Fig.6 Relative activities of different deformation mechanisms of ZK60 alloys along ED (a), 45ED (b), and PED (c)

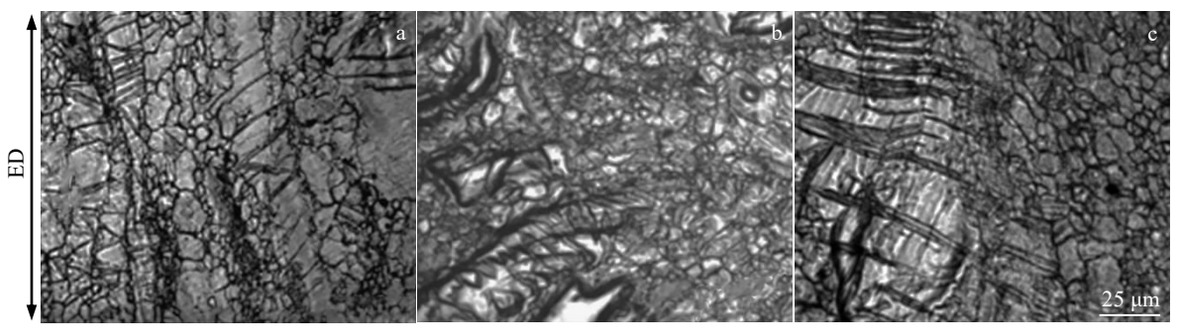

Fig.7 Microstructures of longitudinal section near the fracture surface of ZK60 alloys along ED (a), 45ED (b), and PED (c)

during the simulated tension deformation, so the influence of the pyramidal <*a*> slip is not further discussed.

3 Conclusions

1) When the ZK60 alloy is under tension along the direction perpendicular to the extrusion direction (PED), most of the grains are rotated with a large angle (approximately 90°), which is originated from the {10$\bar{1}$2} twin.

2) For the ZK60 alloy under tension along different directions, the relative activities of deformation mechanisms can well explain the general characteristics of the flow curves, texture evolutions, and the fracture longitudinal microstructures.

3) Prismatic <*a*> slip is the main deformation mode, resulting in the yield asymmetry of ZK60 alloy during tensile deformation along different directions. Due to the preferential orientation, the {10$\bar{1}$1} twin is difficult to initiate and the higher yield strength (287 MPa) can be obtained along the extrusion direction (ED).

4) The preferential orientation distribution of grains causes the yield stress under tension along the direction with an angle of 45° to ED (45ED) higher than that along PED. When the ZK60 alloy is under tension along PED, with increasing the tensile stress, the prismatic <*a*> slip is initiated and gradually increased, resulting in the higher flow curve of ZK60 alloys during tension along PED than that along 45ED at high strains.

References

1 Wu H, Wen S P, Huang H *et al*. *Materials Science and Engineering A*[J], 2016, 651: 415

2 Zhang J H, Liu S J, Wu R Z *et al*. *Journal of Magnesium and Alloys*[J], 2018, 6(3): 277

3 Zuo J R, Hou L G, Shi J T *et al*. *Journal of Alloys and Compounds*[J], 2017, 716: 220

4 Jain J, Poole W J, Sinclair C W. *Scripta Materialia*[J], 2010, 62(5): 301

5 Kurukuri S, Worswick M J, Ghaffari Tari D *et al*. *Philosophical Transactions of the Royal Society A: Mathematical, Physical and Engineering Sciences*[J], 2014, 372(2015): 20 130 216

6 Sun J P, Yang Z Q, Liu H *et al*. *Materials Science and Engineering A*[J], 2019, 759: 703

7 Prasad Y, Rao K P. *Materials Science and Engineering A*[J], 2008, 487(1-2): 316

8 Gehrmann R, Frommert M M, Gottstein G. *Materials Science and Engineering A*[J], 2005, 395(1-2): 338

9 Barnett M R. *Journal of Light Metals*[J], 2001, 1(3): 167

10 Jiang J, Godfrey A, Liu Q *et al*. *Journal of Materials Science & Technology*[J], 2005, 21(12): 1417

11 Jiang J, Godfrey A, Liu W *et al*. *Materials Science and Engineering A*[J], 2008, 483-484: 576

12 Zhou X, Liu R R, Liu Q *et al*. *Metals and Materials International*[J], 2019, 25(5): 1301

13 Chapuis A, Xin Y C, Zhou X J *et al*. *Materials Science and Engineering A*[J], 2014, 612: 431
14 Xin R L, Sun L Y, Liu D J *et al*. *Materials Science and Engineering A*[J], 2014, 602: 1
15 Lu S H, Wu D, Chen R S *et al*. *Materials Science and Engineering A*[J], 2018, 735: 173
16 Koike J, Ohyama R. *Acta Materialia*[J], 2005, 53(7): 1963
17 Agnew S R, Duygulu O. *International Journal of Plasticity*[J], 2005, 21(6): 1161
18 Chapuis A. *Materials Science and Engineering A*[J], 2014, 590: 401
19 Jiang L, Jonas J J, Mishra R K *et al*. *Acta Materialia*[J], 2007, 55(11): 3899
20 Hong S G, Park S H, Lee C S. *Scripta Materialia*[J], 2011, 64(2): 145
21 Khosravani A, Scott J, Miles M P *et al*. *International Journal of Plasticity*[J], 2013, 45: 160
22 Chun Y B, Davies C H J. *Materials Science and Engineering A* [J], 2011, 528(15): 4941
23 Jiang L, Jonas J J, Luo A A. *Materials Science and Engineering A*[J], 2007, 445-446: 302
24 Chang L L, Kang S B, Cho J H. *Materials and Design*[J], 2013, 44: 144
25 Dudamell N V, Ulacia I, Gálvez F *et al*. *Acta Materialia*[J], 2011, 59(18): 6949
26 Begum S, Chen D L, Xu S *et al Materials Science and Engineering A*[J], 2009, 517(1-2): 334
27 Xin Y C, Wang M Y, Zeng Z *et al*. *Scripta Materialia*[J], 2012, 66(1): 25
28 Wu L, Agnew S R, Ren Y *et al*. *Materials Science and Engineering A*[J], 2010, 527(26): 7057
29 Lin X Z, Chen D L. *Materials Science and Engineering A*[J], 2008, 496(1-2): 106
30 Barnett M R. *Materials Science and Engineering A*[J], 2007, 464(1-2): 1
31 Lin J B, Ren W J, Wang X Y *et al*. *Materials Science and Technology*[J], 2016 32(18): 1855
32 Chen Q, Hu L, Shi L X *et al*. *Materials Science and Engineering A*[J], 2020, 774: 138 912
33 Molinari A, Canova G R, Ahzi S. *Acta Metallurgica*[J], 1987, 35(12): 2983
34 Lebensohn R A, Tomé C N. *Acta Metallurgica et Materialia*[J], 1993, 41(9): 2611
35 Lebensohn R A, Tomé C N. *Materials Science and Engineering A*[J], 1994, 175(1-2): 71
36 Kabirian F, Khan A S, Gnäupel-Herlodb T. *International Journal of Plasticity*[J], 2015, 68: 1
37 Tomé C N, Lebensohn R A, Kocks U F. *Acta Metallurgica et Materialia*[J], 1991, 39(11): 2667

基于VPSC仿真的ZK60镁合金拉伸变形行为

周　晨[1]，林金保[1]，何文慧[1]，牟维鹏[2]，刘二强[1]
(1. 太原科技大学 应用科学学院，山西 太原 030024)
(2. 太原科技大学 材料科学与工程学院，山西 太原 030024)

摘　要：通过实验和粘塑性自洽（VPSC）模型，研究了在室温下挤压态ZK60镁合金沿不同方向拉伸时的变形机制开动情况，及其与流动曲线、织构演变和显微组织的对应关系。通过调节VPSC模型的参数，建立了滑移和孪生耦合的晶体塑性力学模型。比较了不同方向拉伸过程中织构演变的差异，分析了变形机制对屈服不对称性的影响。实验和模拟结果表明：当沿垂直于挤压方向（PED）拉伸时，由于{10$\bar{1}$2}孪晶开动，大部分晶粒发生大角度旋转（约90°）。柱面<*a*>滑移是导致ZK60合金沿不同方向拉伸时出现明显屈服不对称的主要变形机理。当ZK60合金沿挤压方向（ED）拉伸时，由于晶粒的择优取向分布，{10$\bar{1}$1}孪晶难以开动，导致ZK60挤压态镁合金拉伸屈服强度较高。ZK60镁合金沿着与ED成45°的方向拉伸时，屈服应力高于沿PED拉伸，但随着拉应力逐渐增大，由于沿PED拉伸时柱面<*a*>滑移逐渐开动，沿PED应变后期的应力曲线逐渐高于沿与ED成45°方向应变的应力曲线。

关键词：ZK60镁合金；粘塑性自洽（VPSC）模型；屈服不对称；变形机制；拉伸

作者简介：周　晨，男，1996年生，硕士生，太原科技大学应用科学学院，山西 太原 030024，E-mail：S20190131@stu.tyust.edu.cn